J. Biochem. 2009;146(3)317–325
doi:10.1093/jb/mvp075

NMR Structure of the Heterodimer of Bem1 and Cdc24 PB1 Domains from *Saccharomyces Cerevisiae*

Kenji Ogura[1,*], Tsubasa Tandai[1,*], Sosuke Yoshinaga[1,*], Yoshihiro Kobashigawa[1], Hiroyuki Kumeta[1], Takashi Ito[2], Hideki Sumimoto[3] and Fuyuhiko Inagaki[1,†]

[1]Department of Structural Biology, Graduate School of Pharmaceutical Sciences, Hokkaido University, Kita 12 Nishi 6, Kita-ku, Sapporo 060-0812; [2]Department of Computational Biology, Graduate School of Frontier Sciences, University of Tokyo, 5-1-5 Kashiwanoha, Kashiwa 277-8561; and [3]Graduate School of Medical Sciences, Kyushu University, 3-1-1 Maidashi, Higashi-ku, Fukuoka 812-8582, Japan

Received April 2, 2009; accepted April 30, 2009; published online May 18, 2009

Bem1 and Cdc24 of the budding yeast *Saccharomyces cerevisiae* interact with each other through PB1–PB1 heterodimer formation to regulate the establishment of cell polarity. Here we present the tertiary structure of the heterodimer of Bem1 and Cdc24 PB1 domains determined by NMR spectroscopy. To avoid ambiguity in the NMR spectral analysis, we first prepared a mutant of the Cdc24 PB1 domain that had truncated loops. The mutant provided well dispersed spectra without spectral overlapping, thus allowing unambiguous spectral assignments for structure determination. We confirmed that the loop deletion-mutant was quite similar to the wild-type in both 3D structure and binding affinity. The NMR structure of the heterodimer of the deletion-mutant of Cdc24 PB1 and Bem1 PB1 was determined using a variety of isotope labelled samples including perdeuteration. The interface between the Bem1/Cdc24 PB1 heterodimer was analysed at atomic resolution. Through a comparison with the tertiary structures of other PB1–PB1 heterodimers, we found that conserved electrostatic properties on the molecular surface were commonly used for PB1–PB1 interaction, but hydrophobic interactions were important for cognate interaction in Bem1/Cdc24 PB1 heterodimer formation.

Key words: Bem1, Cdc24, PB1 domain, heterodimer, NMR, perdeutration, residual dipolar coupling, solution structure.

Abbreviations: Bem1, Bud emergence mediator 1; Cdc24, Cell division control protein 24; PB1, Phox and Bem homology 1; OPCA, OPA, PC and AID; PAR6, partitioning defective 6; phox, phagocyte oxidase; PKC, Protein kinase C; NBR1, neighour of Brca1 gene 1; GST, glutathione S-transferase; NOESY, Nuclear Overhauser enhancement spectroscopy; RDC, residual dipolar coupling; IPAP-HSQC, In-phase and anti-phase heteronuclear single quantum coherence spectroscopy.

The establishment of cell polarity is a crucial step in a variety of biological processes in both single-cell and multicellular organisms. The polarized assembly of the actin and microtubule cytoskeletons is essential for the establishment of cell polarity and depends on site-specific activation of Rho-type GTPases and many critical downstream effectors. In the budding yeast *Saccharomyces cerevisiae*, a scaffold protein Bem1, which tethers a small GTPase Cdc42 and its guanine nucleotide exchange factor (GEF) Cdc24, appears to play an essential role in the establishment of cell polarity during budding in vegetative growth and cell type-specific pheromone-directed mating (*1*). Bem1 mutant proteins that cannot recruit Cdc24 at the site of polarized growth have defects in apical bud growth and mating projection formation (*2*, *3*).

Both Bem1 and Cdc24 possess a PB1 domain at the C terminus. The PB1 domain, originally identified in Phox and Bem1, is a modular domain mediating protein–protein interactions in a variety of biological events through homo- or hetero-dimerization (*4–6*). The PB1 domain is classified into two types; type I (or A, acidic) and type II (or B, basic). The PB1-mediated complex is formed through the interaction between the type I and type II PB1 domains. The type I PB1 domains, such as those of Cdc24, $p40^{phox}$ and PKCι, have a negatively charged acidic region called an OPCA motif (*4*), whereas the type II PB1 domains, including those of Bem1, $p67^{phox}$ and PAR6, have a highly conserved lysine residue. The OPCA motif of the type I PB1 domain specifically interacts with the lysine residue of the type II PB1 domain. Type I/II domains, which present the characteristics of both type I and type II, are also found and potentially form homo oligomerization.

A number of crystal and NMR structures of PB1 domains in monomeric form have been reported, including those of Bem1 (*7*), Cdc24 (*8*), PKCι (*9*), NBR1 (*10*) and MEKK3 (*11*). On the other hand, the structures of PB1 heterodimers have been only reported for $p67^{phox}$/$p40^{phox}$ (*12*) and PAR6/PKCι (*13*). All the PB1 domains

*These authors contributed equally to this work.
†To whom correspondence should be addressed. Tel: +81-11-706-9011, Fax: +81-11-706-9012, E-mail: finagaki@pharm.hokudai.ac.jp

show a ubiquitin-like β-grasp fold topology and consist of two α helices and a five-stranded β sheet with a 2-1-5-3-4 strand order. In the type I PB1 domains, the OPCA motif forms a compact ββα fold in which the three conserved acidic residues in Asp-X-(Asp/Glu)-Gly-Asp adopt a β-turn, leading to the formation of an acidic surface. In the type II PB1 domains, the highly conserved lysine residue is located on the center of the β1 strand. The PB1 heterodimeric structures of $p67^{phox}$/$p40^{phox}$ and PAR6/PKCι showed that heterodimer assembly entails specific electrostatic interactions involving the OPCA motif from the type I PB1 domain and the conserved lysine residue from the type II PB1 domain in a front-to-back manner. Moreover, a second electrostatic interaction was observed in both the $p67^{phox}$/$p40^{phox}$ and PAR6/PKCι complexes. In the $p67^{phox}$/$p40^{phox}$ structure, the C terminal region of the $p40^{phox}$ PB1 domain additionally interacts with the $p67^{phox}$ PB1 domain.

Although the crystal structures of the PB1 heterodimer of $p67^{phox}$/$p40^{phox}$ and PAR6/PKCι have been reported, the mechanism by which each PB1 domain specifically recognizes its cognate partner remains elusive. Here we report the NMR structure of the Bem1/Cdc24 PB1 heterodimer and reveal the mechanism of the specific interaction of the cognate PB1–PB1 complex. To determine the structure of the Bem1/Cdc24 PB1 heterodimer using NMR spectroscopy, we prepared a flexible loop-deletion mutant for unambiguous spectral analysis and a perdeuterated protein for selective detection of intermolecular NOE correlations, thus facilitating high-resolution structure determination of the Bem1/Cdc24 PB1 heterodimer.

MATERIALS AND METHODS

Plasmid Construction—Bem1 (478–551) and Cdc24 PB1 (761–854) genes were amplified by PCR and cloned into a pGEX-6P-1 vector (GE Healthcare, UK) as a GST-fusion protein. The Cdc24 PB1 mutant for amino-acid deletion of ^{770}NNSNNTSS^{777} from the loop-1 and ^{807}NNN^{809} from the loop-2 regions (named Cdc24 PB1DM) was amplified by PCR-mediated site-directed mutagenesis, and cloned into a pGEX-6P-1 vector. The identity of the all constructs was verified by sequencing.

Protein Sample Preparation—Proteins were expressed in *E. coli* strain BL21(DE3) cells. For the unlabelled protein, the transformed cells were grown in Luria–Bertani media. For the preparation of ^{13}C/^{15}N- or ^{15}N-labelled proteins, cells were grown in M9 media containing $^{15}NH_4Cl$ (1 g/l), Celtone-CN or -N (Cambridge Isotope Laboratories, USA) powder (1 g/l), and [U-^{13}C] glucose (2 g/l) or unlabelled glucose. Uniformly ^{15}N/^{2}H-labelled protein was prepared by culturing cells in 100% $^{2}H_2O$ M9 medium using $^{15}NH_4Cl$ and [U-^{2}H] glucose as the sole nitrogen and carbon sources. Cells were grown at 37°C. Protein expression was induced at $OD_{600} = 0.4$ by the addition of isopropyl-1-thio-β-galactopyranoside to a final concentration of 0.4 mM at 25°C. The induced cells were cultured at 25°C for 16 h.

For preparation of Bem1 PB1, the disrupted cell lysate was purified by affinity chromatography using glutathione–sepharose 4B resin (GE Healthcare). The GST tag was removed by incubation for 12 h at 4°C with PreScission Protease (GE Healthcare). The isolated protein was purified by Resource S (GE Healthcare) cation exchange chromatography, followed by gel filtration on a Superdex 75 column (GE Healthcare). Cdc24 PB1 was prepared as described previously (*8*). Cdc24 PB1DM was also purified using the same protocol. For preparation of the Bem1/Cdc24 PB1 heterodimer, purified Bem1 PB1 and Cdc24 PB1DM were mixed at a molar ratio of 1:1, and the protein complex was then purified by gel filtration on a Superdex 75 column with a running buffer containing 50 mM phosphate buffer (pH 6.0), 150 mM NaCl and 0.05% NaN_3.

In Vitro Pull-Down Binding Assay Using Purified Protein—Purified Cdc24 PB1 or PB1DM protein (0.05 mM each) was incubated with purified GST fusion Bem1 PB1 (0.05 mM) in phosphate-buffered saline at 4°C for 1 h. The protein mixture was applied to glutathione–sepharose 4B gel. After washing three times, bound protein was eluted by 15 mM glutathione containing the buffer. The eluate was subjected to 4–12% gradient Bis–Tris NuPAGE gel (Invitrogen, USA) and stained with Coomassie Brilliant Blue. To estimate the amounts of protein on the gel, densitometry analysis was carried out using NIH Image-J software.

NMR Spectroscopy—NMR samples contained 1.0 mM Cdc24 PB1DM and Bem1/Cdc24 PB1 heterodimer. The buffer system consisted of 50 mM phosphate buffer (pH 6.0), 150 mM NaCl and 0.05% NaN_3 in 90% H_2O/10% $^{2}H_2O$ solution. All NMR experiments were run on Inova 800, 600 or 500 MHz NMR spectrometers (Varian, USA) at 25°C, using a triple resonance probe equipped with a Z-axis pulse field gradient coil. A cryogenic probe was used for the experiments run on the Inova 600 MHz spectrometer.

For assignment of ^{1}H, ^{13}C and ^{15}N resonances, a standard suite of heteronuclear NMR spectra were acquired using Protein Pack pulse sequences (Varian) with an isotope-labelled protein. To collect the distance restraints, ^{15}N- and ^{13}C-edited NOESY spectra were measured with a mixing time of 75 ms. Intermolecular NOEs were obtained from a 3D [F_1] ^{13}C-edited, [F_3] ^{13}C-filtered NOESY experiment (*14*) with a mixing time of 75 ms and a 3D ^{15}N-edited NOESY experiment with a mixing time of 200 ms on uniformly ^{13}C/^{15}N-labelled Cdc24 PB1DM and ^{15}N/^{2}H-labelled Cdc24 PB1DM complexed with the non-labelled Bem1 PB1 domain, respectively.

RDCs were collected for a solution containing 1.0 mM uniformly ^{15}N-labelled Bem1/Cdc24 PB1 heterodimer in a liquid crystalline medium consisting of 5% polyethylene glycol/hexanol ($r = 0.96$) (*15*). One-bond ^{1}H-^{15}N coupling constants were measured on an Inova 800 MHz spectrometer at 25°C with IPAP-HSQC experiments (*16*). NMR data were processed using NMRPipe (*17*) and analysed using Sparky (*18*).

Structure Calculation—The cross-peak intensities on the NOESY spectra were integrated using Sparky. Backbone dihedral angle restraints (ϕ and ψ) were predicted by TALOS (*19*). Structures were calculated using Cyana version 2.0 (*20*) using distance, hydrogen bond and dihedral angle restraints, and further refinement

was performed using CNS version 1.1 (*21*) supplemented with RDCs for the PB1 heterodimer. Ramachandran plots were analysed using Procheck-NMR (*22*). Molecular figures were generated by PyMol (DeLano Scientific, USA).

RESULTS AND DISCUSSION

Structure of a Loop Deletion-Mutant of the Cdc24 PB1 Domain—Yoshinaga *et al*. determined the structure of the Cdc24 PB1 domain using NMR and showed that the OPCA motif interacts with the Bem1 PB1 domain by mutagenesis study (*8*). The NMR structure of the Cdc24 PB1 domain (*8*) shows two highly flexible loop regions that are absent in other PB1 domains, leading to overlapping signals in the NMR spectra. We expected that these regions would result in ambiguities in the spectral analysis of the PB1–PB1 heterodimer. The flexible loop regions of the Cdc24 PB1 domain are located on the opposite side to the OPCA motif and were not expected to be involved in the interaction with the Bem1 PB1 domain. Therefore, we prepared a loop deletion-mutant of the Cdc24 PB1 domain in which we deleted the amino-acid sequences ^{770}NNSNNTSS^{777} and ^{807}NNN^{809} from the loop-1 and loop-2 regions, respectively.

Assignment of ^{1}H, ^{13}C and ^{15}N NMR resonances of the loop deletion- mutant of the Cdc24 PB1 domain (Cdc24 PB1DM) was accomplished through the analysis of a suite of NMR spectra described in MATERIALS AND METHODS. Compared with those of the wild-type, the signals of the ^{1}H-^{15}N HSQC spectrum of Cdc24 PB1DM were more highly dispersed (Supplementary Fig. S1). Thus, spectral analysis of Cdc24 PB1DM was less ambiguous than that of the wild-type. First, the structure of Cdc24 PB1DM alone was calculated on the basis of 1861 NOE-derived interproton distance, 124 dihedral angle and 20 hydrogen bond restraints. A total of 100 structures were calculated, and the 20 lowest energy structures were selected. For residues apart from the N-terminal protease cleaved site and flexible loop regions, the root mean square deviation values from the mean structure were 0.44 Å for backbone N, C^{α} and C′, and 0.98 Å for heavy atoms, indicating that the structure of Cdc24 PB1DM was well defined, as illustrated in Fig. 1A. The number of experimental restraints and the structural statistics are summarized in Table 1. The topology of Cdc24 PB1DM is very similar to that of the wild-type Cdc24 PB1 domain. As illustrated in Fig. 1B, the structure consists of secondary structure elements from the N-terminus to the C-terminus; Ile762-Tyr768 (β1), Glu779-Val785 (β2), Phe791-Ile802 (α1), Ile816-Gln819 (β3), Phe825-Leu828 (β4), Asp831-Ala842 (α2) and Phe848-Leu853 (β5). The five β strands form a mixed β-sheet. The inner two strands, β1 and β5, are parallel, while the other strands run in an anti-parallel manner. These are the same as in the NMR structure of the wild-type Cdc24 PB1 domain.

Structural Comparison Between Cdc24 PB1DM and the Wild-Type—The OPCA motif of the Cdc24 PB1 domain consists of the amino-acid region from Ile813 to Met840. To confirm that the loop-deletion mutation did

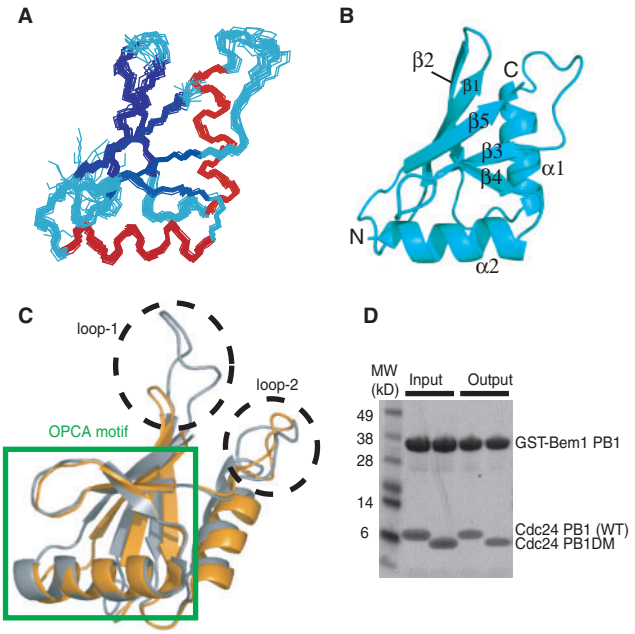

Fig. 1. **(A) Overlay of the 20 lowest energy structures of Cdc24 PB1DM.** Structures are superimposed by least square fit to average N, C^{α} and C′ coordinates of residues 761–766, 779–804 and 813–853. (B) Ribbon model of the averaged structure of Cdc24 PB1DM. The regular secondary structural elements are labelled. (C) Superposition of the wild-type Cdc24 PB1 domain (grey) and PB1DM (orange). The structures are fitted to residues 813–840 containing the OPCA motif. The deleted loop regions and the OPCA motif are enclosed by dashed circles and green lines, respectively. (D) Mutational effect of the binding of Cdc24 PB1 to Bem1 PB1. GST-Bem1 PB1 was incubated with the wild-type Cdc24 PB1 and Cdc24 PB1DM. Proteins pulled down with Glutathione–Sepharose 4B resin were subjected to SDS-PAGE and stained with Coomassie Brilliant Blue.

Table 1. **Structure calculation restraints and structural statistics for Cdc24 PB1DM.**

Number of experimental restraints	
NOE upper distance restraints	
Short-range ($\|i-j\| \leq 1$)	978
Medium-range ($1 < \|i-j\| < 5$)	363
Long-range ($\|i-j\| >= 5$)	520
Total	1,861
Dihedral angle restraints (ϕ and ψ)	124
Hydrogen bonds restraints	20
CYANA structural statistics	
Targen function value (Å^2)	0.14
Root mean square deviation from the averaged coordinates (Å)[a]	
Backbone atoms (N, C^{α}, C′)	0.44
Heavy atoms	0.98
Ramachandran analysis	
Residues in most favoured region	80.2%
Residues in additional favoured region	18.9%
Residues in generously favoured region	0.8%
Residues in disallowed region	0%

[a]For residues 761–768, 779–802 and 813–853.

not change the tertiary structure of the OPCA motif, the NMR structures between the wild-type Cdc24 PB1 domain (in gray) and Cdc24 PB1DM (in orange) were compared (Fig. 1C). The structures of the loop-1 and loop-2 regions were extremely shortened by the mutation; however, the overall structure of the PB1 domain, particularly around the OPCA motif, was not affected by the deletion of the loop regions. The root mean square deviation of C^{α} atoms in the OPCA motif region for Cdc24 between wild-type PB1 and PB1DM was 0.64 Å; therefore, Cdc24 PB1DM was supposed to retain heterodimerization activity with Bem1 PB1.

Binding Affinity of Cdc24 PB1DM to the Bem1 PB1 Domain—Although the structural analysis of Cdc24 PB1DM suggests that the OPCA motif of Cdc24 PB1DM can, in principle, interact with the Bem1 PB1 domain, it is necessary to confirm whether the deletion of the loop regions in Cdc24 PB1DM has any effect on the binding affinity to Bem1 PB1. Thus, the binding affinities of Cdc24 PB1DM and wild-type Cdc24 PB1 to Bem1 PB1 were studied by *in vitro* pull-down binding assay (Fig. 1D). The binding affinity of Cdc24 PB1DM to Bem1 PB1 was similar ($107 \pm 20\%$) to that of the wild-type Cdc24 PB1 domain. It is also to be noted that not only wild-type Cdc24 PB1 but also PB1DM were not dissociated with Bem1 PB1 by the gel filtration experiments running at micromolar concentration. We, therefore, concluded that the loop deletion of the Cdc24 PB1 domain has essentially no effect on binding to the Bem1 PB1 domain and the K_d values were estimated to submicromolar range.

Structure Determination of the Bem1 PB1/Cdc24 PB1DM Heterodimer—To extract reliable inter- and intramolecular correlations from the PB1 heterodimer, we prepared the following three samples for the NMR structural analysis: $^{13}C/^{15}N$-labelled Cdc24 PB1DM complexed with non-labelled Bem1 PB1 (Sample A), non-labelled Cdc24 PB1DM complexed with $^{13}C/^{15}N$-labelled Bem1 PB1 (Sample B) and $^{2}H/^{15}N$-labelled Cdc24 PB1DM complexed with non-labelled Bem1 PB1 (Sample C). The ^{1}H, ^{13}C and ^{15}N resonance assignments of the heterodimer were accomplished with a standard suite of 3D NMR experiments using Sample A and B for Cdc24 and Bem1, respectively. Intramolecular NOE correlation was obtained by standard ^{13}C-edited and ^{15}N-edited NOESY experiments with 75 ms mixing time for both Sample A and Sample B. To detect intermolecular NOE correlations between Bem1 PB1 and the ^{13}C-attached proton of Cdc24 PB1DM, a 3D $[F_1]$ ^{13}C-edtied, $[F_3]$ ^{13}C-filtered NOESY (*14*) experiment was performed for sample A with a mixing time of 75 ms. Perdeuterated proteins are useful for the selective detection of intermolecular NOE correlations between isotope-labelled proteins and non-labelled ligands (*23*). Thus, a 3D ^{15}N-edited NOESY experiment with 200 ms mixing time for Sample C was performed to obtain the intermolecular NOE correlations between Bem1 PB1 and the ^{15}N-attached proton of Cdc24 PB1DM. Unambiguous assignment of intermolecular NOE correlations were obtained as is shown in Supplementary Fig. S2 without overlap of intramolecular NOE cross peaks.

Table 2. **Initial structure calculation restraints and structural statistics for the Bem1/Cdc24 PB1 heterodimer.**

Number of experimental restraints	
NOE upper distance restraints	
Short-range ($\|i-j\| \leq 1$)	1,750
Medium-range ($1 < \|i-j\| < 5$)	631
Long-range ($\|i-j\| \geq 5$)	886
Total	3,267
Dihedral angle restraints (ϕ and ψ)	124
Hydrogen bonds restraints	39
CYANA structural statistics	
Targen function value (Å^2)	0.50
Root mean square deviation from the averaged coordinates (Å)[a]	
Backbone atoms (N, C^{α}, C′)	
Bem1	0.35
Cdc24	0.58
Complex	0.77
Heavy atoms	
Bem1	0.80
Cdc24	1.10
Complex	1.15
Ramachandran analysis	
Residues in most favoured region	75.2%
Residues in additional favoured region	24.2%
Residues in generously favoured region	0.5%
Residues in disallowed region	0%

[a]For residues 477–550 (Bem1) and 761–768, 779–802 and 813–853 (Cdc24).

The initial structure of the Bem1 PB1/Cdc24 PB1DM heterodimer, which we hereafter refer to as the Bem1/Cdc24 PB1 heterodimer, was calculated on the basis of 3267 NOE-derived interproton distance, 124 dihedral angle, 39 hydrogen bond restraints and 10 unambiguous intermolecular distance restraints derived from the ^{13}C-filtered NOESY (Sample A) and ^{15}N-edited NOESY (Sample C) using CYANA software (*20*). A total of 100 structures were calculated, and the 20 lowest energy structures were selected as the initial structure (Supplementary Fig. S3). The number of experimental restraints and the structural statistics are summarized in Table 2. In the initial structure, root mean square deviation from the averaged structure of the heterodimer was 0.76 Å for the backbone atoms excluding the N-terminus and the flexible loop regions. However, individual PB1 domains in the molecular complex were well defined at 0.35 Å resolution for Bem1 and 0.58 Å resolution for Cdc24, suggesting that the interface of the two PB1 domains in the Bem1/Cdc24 heterodimer were not well-defined due to a lack of structural information. Thus, based on the initial structure, 45 intermolecular distance restraints were obtained through the analysis of NOESY spectra of both Sample A and Sample B. Furthermore, domain orientation was refined using 109 RDC data as additional restraints by CNS (*21*). The refined structure of the Bem1/Cdc24 PB1 heterodimer is shown in Fig. 2A, and the number of experimental restraints and the structural statistics are summarized in Table 3.

Structure of the Bem1/Cdc24 PB1 Heterodimer—A stereo view of the superposition of the backbone of

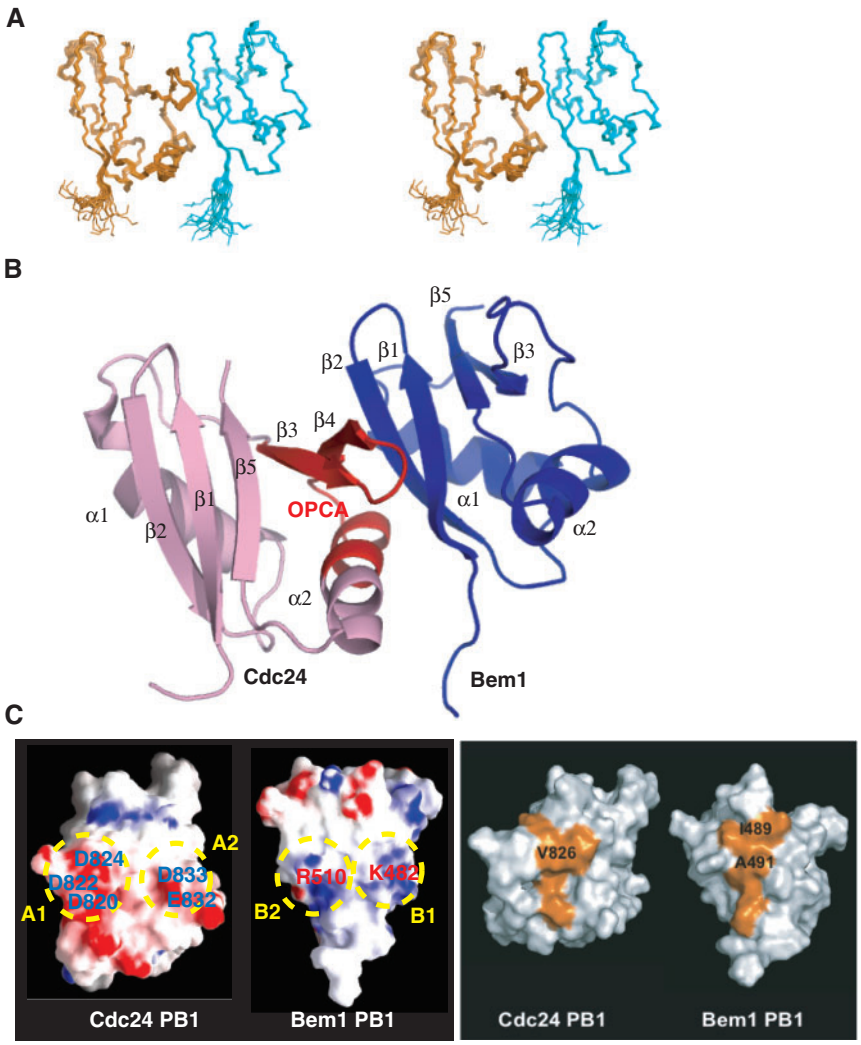

Fig. 2. **(A) A stereo view of the overlay of the backbone heavy atoms (N, C^{α} and C′) of the 20 lowest energy structures of the Bem1/Cdc24 PB1 heterodimer.** The backbones of Cdc24 and Bem1 are coloured orange and cyan, respectively. (B) A schematic representation of the Bem1/Cdc24 PB1 heterodimer. The regular secondary structural elements are labelled. Bem1 and Cdc24 are rendered as blue and pink ribbons, respectively. The OPCA motif region of Cdc24 PB1 is highlighted in red. (C) Molecular surface of the dimeric interface of the Bem1/Cdc24 PB1 heterodimer. The left panel shows the electrostatic surface potentials. The conserved acidic regions of the Cdc24 PB1 domain, A1 and A2, are coloured red and circled in yellow. The conserved basic regions of the Bem1 PB1 domain, B1 and B2, are coloured blue and circled. The right panel shows the hydrophobic clusters that participate in the hydrophobic interaction in orange.

the Bem1/Cdc24 PB1 heterodimer from the 20 lowest energy structures is shown in Fig. 2A. The root mean square deviation values from the mean structure were 0.24 Å for the backbone N, C^{α} and C′, and 0.69 Å for the heavy atoms excluding the N-terminus and flexible loop regions. Refinement using RDC data was extremely helpful to determine the relative orientation of the two domains in the interface. Figure 2B shows a ribbon diagram of the mean structure of the Bem1/Cdc24 PB1 heterodimer. Each PB1 domain in the heterodimer has a similar structure to that observed in its monomeric state (RMSD for Cdc24 and Bem1 are 1.37 Å and 1.17 Å, respectively in Supplementary Fig. S4). Accordingly, we concluded that neither PB1 domain showed any significant conformational change upon dimer formation. Hirano *et al*. have also reported that dimerization of PAR6 and PKCι PB1 domains had no effect on the overall conformation of the each molecule (*9*). Thus, the absence of conformational change on dimerization is appeared to be a general feature of PB1 domains.

Interface of the Bem1/Cdc24 PB1 Heterodimer—The Bem1 and Cdc24 PB1 domains form an asymmetric heterodimer with each PB1 domain using a different face (Fig. 2B). The interface of Cdc24 PB1 is the OPCA motif corresponding to β3, β4 and α2, whereas that of Bem1 PB1 is composed of β1, β2 and the C-terminal region of α1. Thus, Bem1 plays a role as a type II PB1 domain and Cdc24 acts as a type I PB1 domain, as previously reported on the basis of mutational and structural analyses (*7*, *8*). It is noteworthy that the OPCA motif of the

Table 3. **Final structure calculation restraints and structural statistics for the Bem1/Cdc24 PB1 heterodimer.**

	Bem1	Cdc24	Inter-molecular
Number of experimental restraints			
Distance restraints			
Total NOE	1,895	1,607	
Intra-residue	450	427	
Inter-residue			
Sequential ($\|i-j\|=1$)	493	447	
Medium-range ($\|i-j\|<=4$)	359	336	
Long-range ($\|i-j\|>5$)	593	397	55
Hydrogen bonds	42	66	
Total dihedral angle restraints	105	114	
ϕ	52	57	
ψ	53	57	
Total RDCs	59	50	
CNS structural statistics			
Violations			
Distance restraints (Å)	0.017 ± 0.000		
Dihedral angle restraints (°)	0.124 ± 0.046		
Max. dihedral angle violation (°)	4		
Max. distance restraints violation (Å)	0.2		
Deviations from idealized geometry			
Bond lengths (Å)	0.00323 ± 0.00006		
Bond angles (°)	0.598 ± 0.004		
Impropers (°)	0.481 ± 0.018		
Root mean square deviation from the averaged coordinates (Å)[a]			
Backbone atoms (N, C^{α}, C′)			
Bem1	0.14		
Cdc24	0.19		
Complex	0.24		
Heavy atoms			
Bem1	0.58		
Cdc24	0.73		
Complex	0.69		
Ramachandran analysis			
Residues in most favoured region	76.4%		
Residues in additional favoured region	19.2%		
Residues in generously favoured region	1.8%		
Residues in disallowed region	1.8%		

[a]For residues 477–550 (Bem1) and 761–768, 779–802 and 813–853 (Cdc24).

Cdc24 PB1 domain is responsible for the interaction with the Bem1 PB1 domain, but no other regions are used for dimerization.

The electrostatic surface potential of the interface between the Bem1/Cdc24 PB1 heterodimer is shown in Fig. 2C left. The Cdc24 PB1 domain presents two acidic regions, A1 (Asp820, Asp822 and Asp824) and A2 (Glu832 and Asp833), whereas Bem1 PB1 presents two basic regions, B1 (Lys482) and B2 (Arg510). The complementarity of the surface potential between A1–B1 and A2–B2 supports the notion that electrostatic interaction plays an important role in Bem1/Cdc24 PB1 heterodimer formation. In addition, a hydrophobic interaction between Ile489 and Ala491 of Bem1 and Val826 of Cdc24 also contributes to dimerization (Fig. 2C right). Actually, a number of intermolecular NOEs were observed between V826 and Ile489, and Ala491 in the NOESY strip (Supplementary Fig. S2).

Correlation of Structure and Mutagenesis Studies on Bem1/Cdc24 PB1–PB1 Interactions—We have previously reported extensive mutagenesis studies on Bem1 and Cdc24 PB1s using *in vitro* pull-down assays (*7*, *8*). These studies have shown that Cdc24 mutants D820A (A1), D824A (A1) and D833A (A2) have reduced relative binding affinities of less than 10% of that of the wild-type. Furthermore, Bem1 mutants K480A (B1), K482A (B1) and R510A (B2) showed reduced binding affinities of less than 40, 10 and 70%, respectively. In addition, the Cdc24 mutant V826A and Bem1 mutants I489A and A491N have reduced binding affinities of less than 10, 60 and 50%, respectively. Now, we can discuss the results of the mutagenesis studies based on the structure of the Cdc24/Bem1 PB1 heterodimer (Fig. 3 in parentheses).

Figure 3A shows the detailed interaction surface of the Bem1/Cdc24 PB1 heterodimer. Lys482 of Bem1 (B1) is

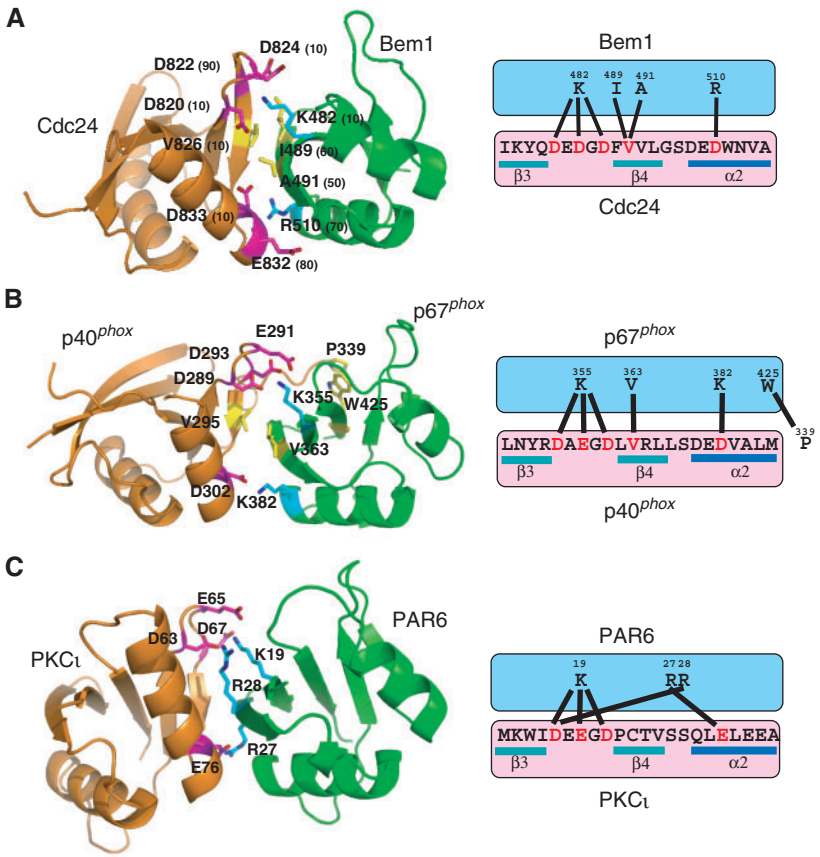

Fig. 3. **Structural comparison among the PB1–PB1 heterodimers of Bem1/Cdc24 (A), p67^{phox}/p40^{phox} (B) and PAP6/PKCι (C).** The structure in the left panel shows the residues involved in the interface. Basic, acidic and hydrophobic residues are coloured blue, red and yellow, respectively. The right panel shows an interaction diagram of the residues of the type-II PB1 domain with residues of the OPCA motif of the type-I PB1 domain. Secondary structure elements are indicated below the Cdc24, p40^{phox} and PKCι sequences. Numbers in parentheses in the left panel of (A) give the relative binding affinities (%) of mutants compared with the wild-type PB1 domains.

surrounded by the acidic residues Asp820, Asp822 and Asp824 of Cdc24 (A1). The Lys482 mutation of Bem1 completely abolished binding to Cdc24 PB1. Thus Lys482, which is highly conserved in type II PB1s, is a key residue for the interaction of Bem1 PB1 with Cdc24 PB1. In Cdc24 PB1, Asp820, Asp822 and Asp824 form an acidic cluster (A1) that fixes the side chain of Lys482. Mutational studies show that Asp820 and Asp824 of Cdc24 are important residues for Bem1 PB1 binding. In particular, the Asp820 mutation abolishes binding to Bem1 PB1. Asp820 and Asp824 are highly conserved residues on the OPCA motif and are generally responsible for binding to type II PB1s. On the other hand, *in vitro* pull-down assay shows that the D822A mutant presents reduced binding affinity to 90% of that of the wild-type (data not shown). Thus, of the three aspartate residues forming the A1 cluster, Asp820 and Asp824 play a critical role in Bem1 PB1 binding, and Asp822 serves to assist the binding. Although K480A mutation of Bem1 decreases binding affinity, the side chain of Lys480 is not proximal to the A1 cluster of Cdc24.

Arg510 of Bem1, which forms the basic B2 cluster, fits into the acidic A2 cluster formed by Glu832 and Asp833 of Cdc24. The mutational studies show that Asp833 is an important residue for the A2–B2 interaction as the D833A mutation decreases the binding affinity to less than 10%. Although the R510A mutation of Bem1 decreases binding affinity to only 70%, Arg510 is conserved in Bem1 homologues and is considered to be a critical residue for binding to the A2 cluster of Cdc24. A recent mutational experiment showed that E832A mutation only reduced binding affinity to 80% of that of the wild-type, as shown by *in vitro* pull-down binding assay (data not shown).

The tertiary structure of the Bem1/Cdc24 PB1 heterodimer shows that the interface consists of not only electrostatic clusters generally used in PB1–PB1 interactions but also a hydrophobic cluster formed by Val826 (Cdc24), Ile489 (Bem1) and Ala491 (Bem1). Mutation of these residues to alanine or asparagine reduced binding affinities between the Bem1 and Cdc24 PB1 domains. According to the present structure, Val826 of Cdc24, the mutation of which decreased the binding affinity to 10%, fits into the hydrophobic pocket formed by Ile489 and Ala491 of Bem1 (Supplementary Fig. S2). Mutation of Ile489 and Ala491 also effectively decreased the binding affinities to around 50%. Thus, this hydrophobic interaction is also important for Bem1/Cdc24 PB1 heterodimer formation.

Comparison with Other PB1 Heterodimer Structures—To date, only two crystal structures of the PB1 heterodimers, $p67^{phox}$/$p40^{phox}$ (*12*) and PAR6/PKCι (*13*) have been reported. Both structural and mutational analyses have shown that the PB1–PB1 interaction is maintained by an electrostatic interaction between the acidic region of type I PB1s and the basic region of type II PB1s. Figure 3B and C show ribbon diagrams and the key residues required for the interaction of the PB1 heterodimer in $p67^{phox}$/$p40^{phox}$andPAR6/PKCι, respectively.

In the $p67^{phox}$/$p40^{phox}$ PB1 heterodimer, Lys355 of $p67^{phox}$ (B1) corresponds to the highly conserved lysine residue in type II PB1s. In fact, Lys355 interacts with three acidic residues, Asp289, Glu291 and Asp293 on the OPCA motif of $p40^{phox}$ (A1) in a manner similar to Lys482 in Bem1. Moreover, there is another electrostatic interaction between Lys382 of $p67^{phox}$ (B2) and Asp302 of $p40^{phox}$ (A2). The sequence alignment of these key residues for dimerization is exactly matched between the Bem1/Cdc24 and $p67^{phox}$/$p40^{phox}$ PB1 heterodimers (Right panel on Fig. 3A and B, respectively). An additional hydrophobic interaction is similarly found at the region sandwiched by the two electrostatic interaction surfaces in the $p67^{phox}$/$p40^{phox}$ heterodimer. The hydrophobic interaction consists of a pairwise interaction maintained by Val363 of $p67^{phox}$ and Val295 of $p40^{phox}$. Although the hydrophobic interaction is very similar to that of the Bem1/Cdc24 PB1 heterodimer, Val826 of Cdc24, which corresponds to Val295 of $p40^{phox}$, binds to both Ile489 and Ala491 of Bem1. As a unique feature of the $p67^{phox}$/$p40^{phox}$ heterodimer, the C-terminal tail of $p40^{phox}$ comes into hydrophobic contact with Trp425 of $p67^{phox}$. Although this interaction has been confirmed by mutational analysis, it is excluded from the canonical PB1 domain interaction because this interaction is not found in other PB1 heterodimers.

In the PAR6/PKCι PB1 heterodimer, the electrostatic interaction of the A1–B1 and A2–B2 clusters is very similar to those of $p67^{phox}$/$p40^{phox}$ and Bem1/Cdc24 PB1 heterodimers; however, there are slight differences in details. Lys19 (B1) of PAR6 binds to the A1 cluster formed by Asp63, Glu65 and Asp67 of PKCι. Additionally, Arg28 in β2 participates in the B1 cluster, and Arg27 in β2 binds to Glu76 in the A2 cluster of PKCι. In the $p67^{phox}$/$p40^{phox}$ and Bem1/Cdc24 PB1 heterodimers, residues involved in β2 of type-II PB1s play a role in hydrophobic, not electrostatic, interactions. Thus, there is no apparent hydrophobic interaction between the PAR6 and PKCι PB1 domains. These features are unique to the PAR6/PKCι PB1 heterodimer.

Recently, the structure of the MEK5/MEKK3 PB1 heterodimer was reported (2O2V), where the electrostatic interactions between A1and B1, and A2 and B2 were observed. In addition, hydrophobic interaction in the interface was present. These features are similar to those in the Cdc24/Bem1 and $p40^{phox}$/$p67^{phox}$ PB1 heterodimers.

CONCLUSION

In the present study, we have determined the tertiary structure of the Bem1/Cdc24 PB1 heterodimer using NMR spectroscopy with a degree of accuracy comparable to those determined by X-ray crystallography. To achieve this, we prepared a loop-deletion mutant of the Cdc24 PB1 domain and confirmed that the mutation does not affect dimerization affinity. We also prepared a set of isotope-labelled heterodimers including perdeuterated proteins to obtain unambiguous assignments of intra- and intermolecular NOE correlations. Finally, to determine the relative orientation of the PB1 domains, RDCs were observed and incorporated into the structural calculation at the final refinement-stage. It should be noted that these methods are useful and generally applicable for the structural determination of protein–protein complexes using high-resolution NMR spectroscopy.

The NMR structure of the Bem1/Cdc24 PB1 heterodimer was compared with the crystal structures of the $p40^{phox}$/$p67^{phox}$ PB1, Par/PKCι PB1 and MEK5/MEKK3 PB1 heterodimers. The Bem1/Cdc24 PB1 heterodimer has two electrostatic interaction surfaces common to the PB1–PB1 heterodimers. However, detailed inspection of the interface of these heterodimers clearly demonstrated that each cognate pair developed specific interactions that endowed specificity.

PDB ACCESSION CODES

The atomic coordinates for the Cdc24 PB1DM and Bem1/Cdc24 PB1 heterodimer have been deposited in the Research Collaboratory for Structural Bioinformatics Protein Data Bank under accession codes 2KFJ and 2KFK, respectively.

SUPPLEMENTARY DATA

Supplementary data are available at *JB* online.

FUNDING

Grant-in-Aid for Scientific Research (Kiban S); the National Projects on Targeted Proteins Research Programs from the Ministry of Education, Science and Culture of Japan.

REFERENCES

1. Pruyne, D. and Bretscher, A. (2000) Polarization of cell growth in yeast. *J. Cell. Sci.* **113**, 571–585
2. Ito, T., Matsui, Y., Ago, T., Ota, K., and Sumimoto, H. (2001) Novel modular domain PB1 recognizes PC motif to mediate functional protein–protein interactions. *EMBO J.* **20**, 3938–3946
3. Butty, A.C., Perrinjaquet, N., Petit, A., Jaquenoud, M., Segall, J.E., Hofmann, K., Zwahlen, C., and Peter, M. (2002) A positive feedback loop stabilizes the guanine-nucleotide exchange factor Cdc24 at sites of polarization. *EMBO J.* **21**, 1565–1576
4. Ponting, C.P., Ito, T., Moscat, J., Diaz-Meco, M.T., Inagaki, F., and Sumimoto, H. (2002) OPR, PC and AID: all in the PB1 family. *Trends Biochem. Sci.* **27**, 10
5. Moscot, J., Diaz-Meco, M.T., Albert, A., and Campuzano, S. (2006) Cell signaling and function organized by PB1 domain interactions. *Mol. Cell* **23**, 631–640
6. Sumimoto, H., Kamakura, S., and Ito, T. (2007) Structure and function of the PB1 domain, a protein interaction

module conserved in animals, fungi, amoebas, and plants. *Sci. STKE* **2007**, re6
7. Terasawa, H., Noda, Y., Ito, T., Hatanaka, H., Ichikawa, S., Ogura, K., Sumimoto, H., and Inagaki, F. (2001) Structure and ligand recognition of the PB1 domain: a novel protein module binding to the PC motif. *EMBO J.* **20**, 3947–3956
8. Yoshinaga, S., Kohjima, M., Ogura, K., Yokochi, M., Takeya, R., Ito, T., Sumimoto, H., and Inagaki, F. (2003) The PB1 domain and the PC motif-containing region are structurally similar protein binding modules. *EMBO J.* **22**, 4888–4897
9. Hirano, Y., Yoshinaga, S., Ogura, K., Yokochi, M., Noda, Y., Sumimoto, H., and Inagaki, F. (2004) Solution structure of atypical protein kinase C PB1 domain and its mode of interaction with ZIP/p62 and MEK5. *J. Biol. Chem.* **279**, 31883–31890
10. Müller, S., Kursula, I., Zou, P., and Wilmanns, M. (2006) Crystal structure of the PB1 domain of NBR1. *FEBS Lett.* **580**, 341–344
11. Hu, Q., Shen, W., Huang, H., Liu, J., Zhang, J., Huang, X., Wu, J., and Shi, Y. (2007) Insight into the binding properties of MEKK3 PB1 to MEK5 PB1 from its solution structure. *Biochemistry* **46**, 13478–13489
12. Wilson, M.I., Gill, D.J., Perisic, O., Quinn, M.T., and Williams, R.L. (2003) PB1 domain-mediated heterodimerization in NADPH oxidase and signaling complexes of a typical protein kinase C with Par6 and p62. *Mol. Cell* **12**, 39–50
13. Hirano, Y., Yoshinaga, S., Takeya, R., Suzuki, N.N., Horiuchi, M., Kohjima, M., Sumimoto, H., and Inagaki, F. (2005) Structure of a cell polarity regulator, a complex between atypical PKC and Par6 PB1 domains. *J. Biol. Chem.* **280**, 9653–9661
14. Ogura, K., Terasawa, H., and Inagaki, F. (1996) An improved double-tuned and isotope-filtered pulse scheme based on a pulsed field gradient and a wide-band inversion shaped pulse. *J. Biomol. NMR* **8**, 492–498
15. Rückert, M. and Otting, G. (2000) Alignment of biological macromolecules in novel nonionic liquid crystalline media for NMR experiments. *J. Am. Chem. Soc.* **122**, 7793–7797
16. Ottiger, M. and Bax, A. (1998) Characterization of magnetically oriented phospholipid micelles for measurement of dipolar couplings in macromolecules. *J. Biomol. NMR* **12**, 361–372
17. Delaglio, F., Grzesiek, S., Vuister, G.W., Zhu, G., Pfeifer, J., and Bax, A. (1995) NMRPipe: a multidimensional spectral processing system based on UNIX pipes. *J. Biomol. NMR* **6**, 277–293
18. Goddard, T.D. and Kneller, D.G. SPARKY 3, University of California, San Francisco, CA., http://www.cgl.ucsf.edu/home/sparky/. Last accessed 30 May 2008
19. Cornilescu, G., Delaglio, F., and Bax, A. (1999) Protein backbone angle restraints from searching a database for chemical shift and sequence homology. *J. Biomol. NMR* **13**, 289–302
20. Güntert, P. (2004) Automated NMR structure calculation with CYANA. *Methods Mol. Biol.* **278**, 353–378
21. Brünger, A.T., Adams, P.D., Clore, G.M., DeLano, W.L., Gros, P., Grosse-Kunstleve, R.W., Jiang, J.S., Kuszewski, J., Nilges, M., Pannu, N.S., Read, R.J., Rice, L.M., Simonson, T., and Warren, G.L. (1998) Crystallography & NMR system: A new software suite for macromolecular structure determination. *Acta. Crystallogr. D Biol. Crystallogr.* **54(Pt 5)**, 905–921
22. Laskowski, R.A., Rullmannn, J.A., MacArthur, M.W., Kaptein, R., and Thornton, J.M. (1996) AQUA and PROCHECK-NMR: programs for checking the quality of protein structures solved by NMR. *J. Biomol. NMR* **8**, 477–486
23. Ogura, K., Shiga, T., Yokochi, M., Yuzawa, S., Burke, T.R. Jr., and Inagaki, F. (2008) Solution structure of the Grb2 SH2 domain complexed with a high-affinity inhibitor. *J. Biomol. NMR* **42**, 197–207